Appl. Phys. A (2016)122:443
DOI 10.1007/s00339-016-9981-2

Applied Physics A
Materials Science & Processing

Thermally chargeable supercapacitor working in a homogeneous, changing temperature field

Hyuck Lim[1] · Yang Shi[1] · Yu Qiao[1,2]

Received: 28 September 2015 / Accepted: 9 March 2016

Abstract A thermally chargeable supercapacitor (TCS) system is developed to harvest electrical energy from a uniform temperature field of a changing low-grade heat source. Without any temperature gradient, the TCS absorbs heat when temperature rises and releases electricity during discharging. As temperature decreases, the system configuration returns to the initial condition, so that the thermal-to-electrical energy conversion can be continuously conducted. With a nickel-coated carbon nanotube or nanoporous carbon-based electrode, the thermal sensitivity and the electrode surface area are enhanced simultaneously, leading to a high output voltage around 100–160 mV and a high specific energy of 600–1800 mJ per gram of electrode material in each thermal cycle, with a mild temperature range of ~50 °C.

1 Introduction

Harvesting thermal energy from low-grade heat (LGH) is an important yet challenging task. The temperature range of LGH is typically from room temperature to 350 °C [1], for which the Carnot cycle limit is low [2]. As a result, the efficiency as well as the cost-performance balance of conventional indirect or direct energy conversion techniques, such as organic Rankine cycle (ORC) machines and thermoelectric materials, is quite poor [3, 4]. Currently, a large amount of LGH is being wasted in the cooling systems of power plants [5], in vehicle engines [6], as geothermal energy [7], among others. It is highly desirable that new technologies of higher efficiency and lower costs can be developed.

In addition to the low energy density, another issue associated with LGH is the difficulty in maintaining a stable temperature gradient. A conventional direct or indirect energy conversion system works between a high-temperature heat source and a low-temperature heat sink [8]. As thermal energy diffuses from the heat source to the heat sink, a portion of the LGH is converted to electric power and the rest is "wasted". In order to keep the temperature difference sufficiently large, very often sophisticated and expensive heat exchangers must be employed. Due to the low energy conversion efficiency and rate, to obtain useful electricity, a large amount of thermal energy must be dissipated; moreover, in many LGH environments, a low-temperature heat sink is hard to maintain [9].

Recently, we developed a capacitive energy harvesting system for LGH: thermally chargeable supercapacitor (TCS) [10–14]. Fundamentally different from conventional direct energy conversion mechanisms, TCS is not based on the Seebeck effect, but on the capacitive effect. In the electric double layer formed at an electrolyte–electrode interface, the ion density and electrode potential change with temperature [13]:

$$\left|\frac{\mathrm{d}V}{\mathrm{d}T}\right| = -\frac{1}{K_{\mathrm{IHP}} \cdot B}\left(k_B \cdot A \cdot \ln c + \frac{\mathrm{d}Q_0}{\mathrm{d}T}\right)$$

where, V, T, K_{IHP}, k_B, c and Q_0 are electrode potential, cell temperature, capacity of inner Helmholtz plane, Boltzmann constant, ion concentration, and heat of adsorption, respectively; A and B are two system constants. $|\mathrm{d}V/\mathrm{d}T|$ can be affected by ion charge and size, electrode material, and solvent [11–14, 22]. In one embodiment, a TCS consists of two

✉ Yu Qiao
yqiao@ucsd.edu

[1] Program of Materials Science and Engineering, University of California - San Diego, La Jolla, CA 92093, USA

[2] Department of Structural Engineering, University of California - San Diego, La Jolla, CA 92093-0085, USA

Published online: 22 March 2016

identical electrodes immersed in an electrolyte solution. The two electrodes are placed at different temperatures, and the electrolyte solutions are connected via a salt bridge. Because the electrode potential is thermally dependent, as the two electrodes are connected together through a resistor, a transient current is generated before the output voltage vanishes, converting a considerable amount of thermal energy to electrical energy. The thermal sensitivity of TCS can be higher than that of thermoelectric materials by more than an order of magnitude. It works best when the temperature is below the boiling point of the solvent, often within the LGH range.

In the above setup, the TCS is placed in between a heat source and a heat sink, similar with conventional energy conversion systems. As the TCS configuration is modified, the same capacitive effect can be employed to harvest thermal energy from a homogeneous, changing temperature field [15]: An electrode and a counter-electrode are sandwiched with a membrane separator and immersed in an electrolyte solution. The temperature is spatially uniform; that is, there does not exist any temperature gradient. However, the temperature is temporally fluctuating between a low temperature, T_r, and a high temperature, T_{max}. At T_r, the electrode and the counter-electrode are grounded and the net output voltage is zero. As temperature changes to T_{max}, because the thermal sensitivities of electrode potentials of different materials are different, an output voltage, V, would be built up. If the two electrodes are connected by a resistor, a transient current is generated, converting heat to electricity. Compared with electrochemical systems [16, 17], the capacitive TCS tends to have a superior cycling performance and a much lower cost [18]. In addition to the thermal sensitivity of output voltage, another important factor that determines the energy density of TCS is the effective surface areas of the electrodes. To investigate its effect, we tested two dissimilar nano-structured materials: Ni-coated carbon nanotube and conductive activated carbon.

For a small-scale compact TCS system, each temperature fluctuation cycle may take only a few seconds [19]; the materials cost of electrodes is typically a few dollars per pound. Thus, to achieve an economically competitive power cost of ~$0.5/W, the specific energy, i.e., the generated electric energy per temperature fluctuation cycle per gram of electrode material, should be ~50 mJ/g, beyond the capability of previously developed systems [e.g., 10]. The current study will be focused on enhancing the specific energy of TCS.

2 Experimental

2.1 Fabrication of energy harvesting cell

Figure 1 depicts the TCS setup. It was a single cell consisting of a container, an electrolyte solution, a working

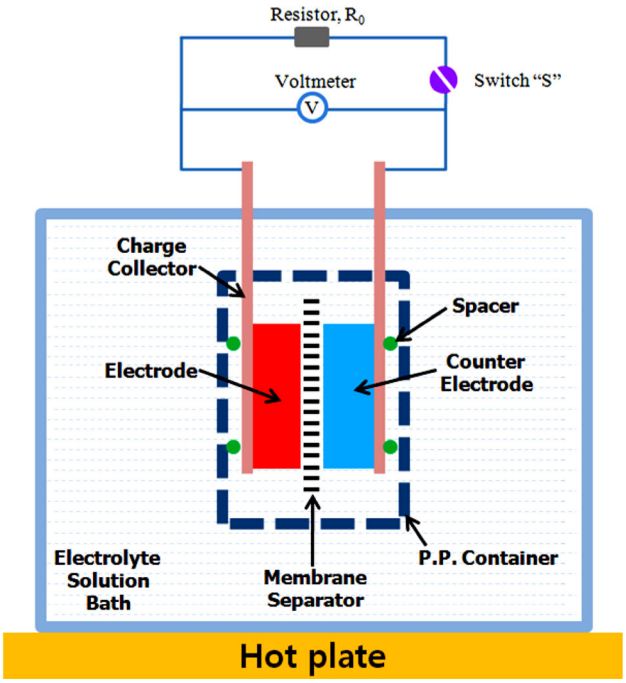

Fig. 1 Schematic of the TCS system

electrode, a counter-electrode, and a membrane separator. The two electrodes and separator were stacked between two platinum charge collectors. The container was a polypropylene (PP) case sealed by Teflon tapes, immersed in an electrolyte bath heated by a hot plate. The electrolyte was 1 M formamide (FA) solution of sodium acetate ($NaC_2H_3O_2$). The boiling point of FA was ~210 °C. In the electrolyte solution, an electrode and a counter-electrode were firmly compressed against a membrane separator from both sides, forming a sandwich structure. PTFE o-rings were used as spacers between the electrodes and the PP case. For better thermal conduction, channels were produced on the PP case. The membrane separator was a Celgard-3510 polypropylene sheet.

2.2 Fabrication of counter-electrode

The counter-electrode was made of a nanoporous carbon, obtained from Cabot (product no. BP2000). It was in the form of ~50-μm large particulates; its specific surface area was 1800 m^2/g; the pore size ranged from 1 nm to 100 nm, with two distribution peaks at ~3 and ~70 nm, respectively [20]. The material was refluxed at 80 °C in acetone for 4 h, collected through filtration, rinsed in distilled water and alcohol repeatedly, and vacuum dried at 80 °C for 12 h. The dry powders were compressed on a thin platinum (Pt) foil by a type 5582 Instron machine at 400 MPa for 5 min, into 10-mm-diameter disks. The mass of each nanoporous carbon disk was around 20 mg. The Pt foil was employed as charge collector.

2.3 Fabrication of working electrode

Two types of electrodes were processed. The first was based on nickel (Ni)-coated Cheap Tubes sku-030102 multiwall carbon nanotubes (MWCNT), with the outer diameter around 8–15 nm and the specific surface area of $\sim$230 m^2/g. The Ni coating was carried out through electroless deposition [21]. The MWCNT was first rinsed by distilled water and then refluxed in a mixture of nitric acid and sulfuric acid for 4 h. The nitric-to-sulfuric acid ratio was 1:3; the mixture was vigorously stirred during refluxing. After filtration and rinsing, the MWCNT was ultrasonically agitated at room temperature for 10 min in an aqueous solution of 0.05 mol/L tin chloride dihydrate ($SnCl_2{\cdot}2H_2O$) and 0.1 M/L chlorine acid (HCl), and at room temperature for 30 min in an aqueous solution of 5.6×10^{-4} mol/L palladium chloride (PdCl2) and 0.12 mol/L chlorine acid; immediately after each step of bathing, the material was collected via filtration and repeatedly rinsed. The first bathing was to activate carboxylic and hydroxyl surface groups; the second bathing was to form palladium catalytic nuclei on the carbon surfaces. Then, the MWCNT was nickel-plated at 80 °C for 24 h in an aqueous electroless bath of 0.05 M nickel chloride hydrate ($NiCl_2{\cdot}6H_2O$), 0.5 M boric acid (H_3BO_3), 0.4 M hydrazine monohydrate ($N_2H_4{\cdot}H_2O$), and 0.5 M gluconic acid ($C_6H_{12}O_7$), with the pH value being adjusted to 12, with vigorous stirring. Here, boric acid and gluconic acid were used for pH control, and hydrazine and gluconic acids were used as reducing and complexing regent for Ni ion, respectively. The coated material was collected through filtration, repeatedly rinsed, and finally, O-containing surface groups on the CNT surface were reduced in a tube furnace in a 5 % hydrogen gas environment at 500 °C for 60 min. We characterized the Ni-coated MWCNT (NiCNT) using a scanning electron microscope (Phillips XL30 ESEM) and the energy dispersive spectroscopy (EDS) equipped in it. Figure 2a, b show typical SEM images of NiCNT and Ni-coated nanoporous carbon (NiNC). Uniform Ni coating was confirmed by the EDS analysis results listed in Table 1. The Ni-coated MWCNT (NiCNT) was compacted into disk form on a thin Pt charge collector foil, by using a type 5582 Instron machine at 400 MPa. The disk diameter was $\sim$10 mm; the electrode mass was around 20 mg.

The second type of electrode was based on Cabot-BP2000 nanoporous carbon, the same as the counter-electrode. The nanoporous carbon was coated by Ni and compressed into disks through a similar electroless deposition procedure as NiCNT, forming Ni-coated nanoporous carbon (NiNC) electrodes.

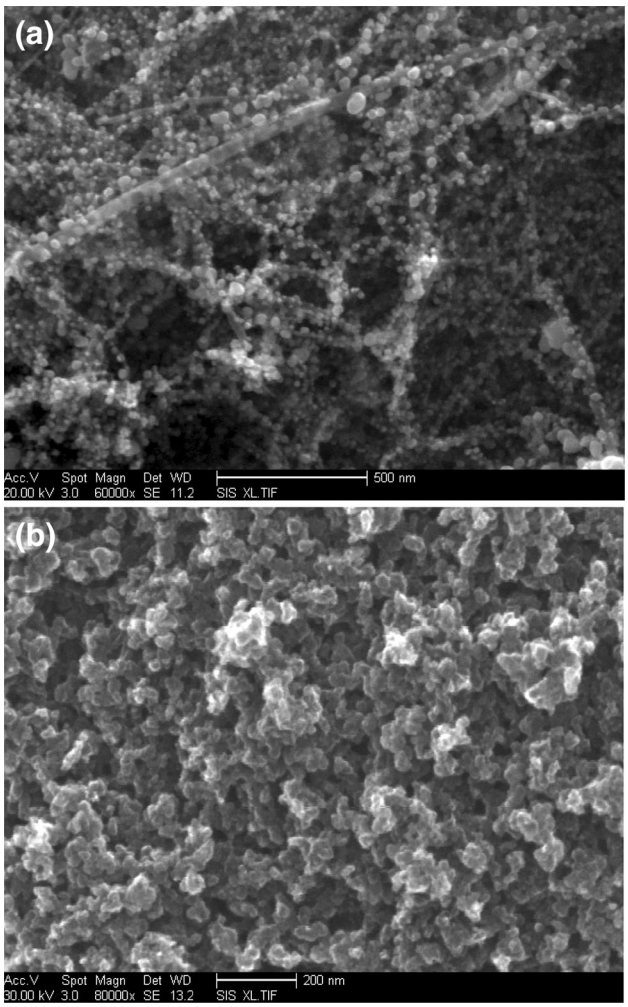

Fig. 2 Typical SEM images of **a** NiCNT and **b** NiNC

Table 1 EDS analysis results of nickel-coated (a) carbon nanotube (NiCNT) and (b) nanoporous carbon (NiNC)

	NiCNT (Atomic %)	NiNC (Atomic %)
C	69.65	83.98
Ni	28.97	4.98
Sn	1.38	0.27
O	0	10.77
Total	100	100

2.4 Measurement setup of energy harvesting performance

Two Pt wires were, respectively, attached to the Pt charge collectors on the electrode and the counter-electrode, and extended out of the TCS cell. An electrical switch "S" and a 1-kΩ resistor "R_0" were placed in series and

connected to the two Pt wires. The switch and the resistor were in parallel with a NI-SCB68 data acquisition (DAQ) system, which was employed to measure the output voltage, V. Inside the cell, a type-K thermocouple was inserted to monitor the cell temperature, T, with a NI HH-20A Reader.

When the switch "S" was open, a Corning PC-220 hot plate heated the TCS cell, causing its temperature to rise from room temperature, T_r, with a rate of about 3 °C/min. The relationship between the open-circuit voltage and the cell temperature is given in Fig. 3. After the peak temperature, T_{max}, was achieved, the cell temperature was maintained constant and the switch "S" was closed. The output voltage over the resistor "R_0" was recorded, as shown in Fig. 4. The temperature change, ΔT, was 45–50 °C. The current across R_0 was transient and would eventually decrease to zero, after which the hot plate was turned off and the TCS cell was cooled down back to room temperature, with the switch "S" remained close. Finally, at T_r, "S" was turned open; the system became identical to its initial configuration and could be operated for the next thermal cycle.

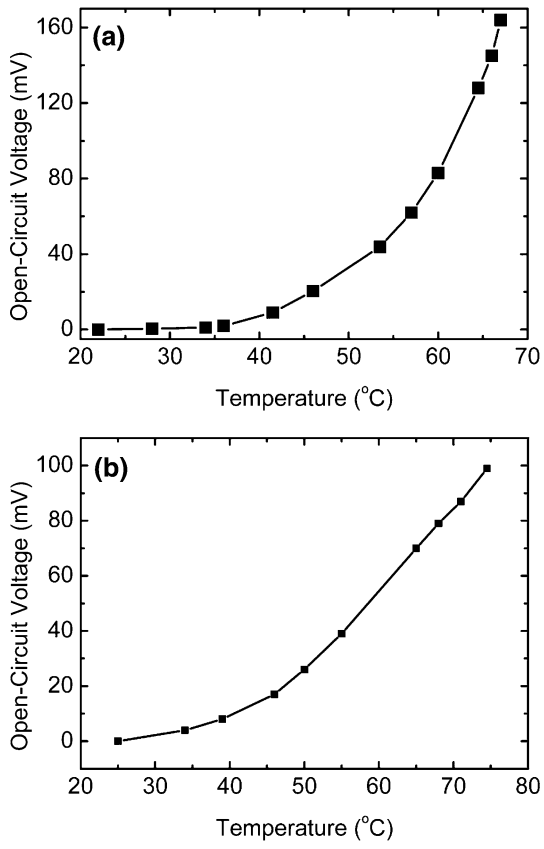

Fig. 3 Typical open-circuit voltage of nickel-coated **a** carbon nanotube and **b** nanoporous carbon, as a function of the low-grade heat (LGH) temperature

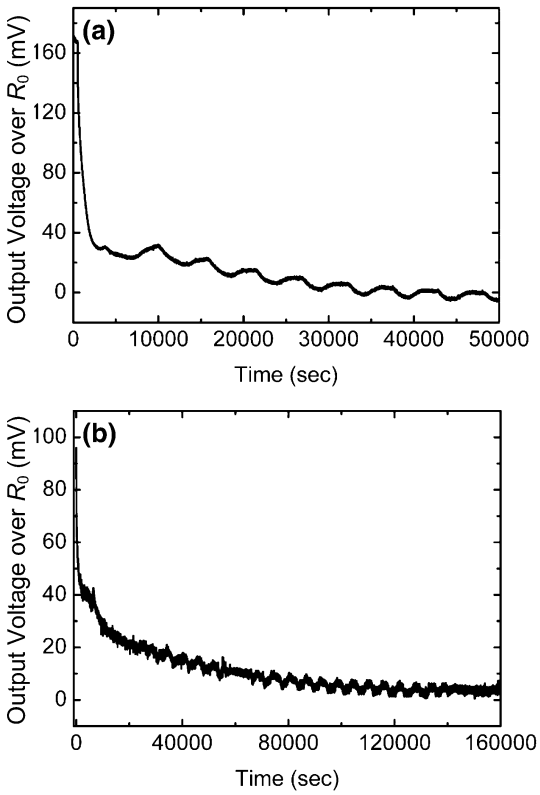

Fig. 4 Typical discharge curves of nickel-coated **a** carbon nanotube and **b** nanoporous carbon

3 Results and discussion

The specific energy of TCS can be evaluated as $E \propto (C{\cdot}A)(\mathrm{d}V/\mathrm{d}T{\cdot}\Delta T)$, where C is the charge density at the electrode–electrolyte interface, A is the specific surface area, and $\mathrm{d}V/\mathrm{d}T$ is the temperature sensitivity of output voltage. Clearly, $\mathrm{d}V/\mathrm{d}T$ and A are two vital factors that govern the performance of the system.

In a previous experimental study [22], we noticed that the thermal sensitivity of electrode potential is highly dependent on the work function (WF) of the electrode material, which fits with the classic jellium model quite well [23]: As the WF rises, due to the increase in positive ion density, n_+, the potential difference across an electrode–electrolyte interface double layer tends to vary significantly with temperature, even though the contributions from the capacitive effects of Helmholtz layer and diffusion layer may be negligible. Among many electrically conductive materials, Ni has a relatively high WF value, 5.2 eV [24] and a relatively low cost, and thus, is chosen as the electrode material. In order to also achieve a large specific surface area, A, carbon nanotubes and nanoporous carbon are employed as substrates. As they are coated, Ni can be fully exposed to the electrolyte solution, leading to a large capacitance [25].

According to Fig. 3, the open-circuit TCS voltage, V, is nonlinear to the cell temperature, T. For the NiCNT cell, as temperature rises from room temperature, $T_r \approx 22$ °C, to about 40 °C, the potential difference between the electrode and the counter-electrode is only a few mV; the value of dV/dT is comparable with the Seebeck coefficients of many thermoelectrics [26].When the temperature change, ΔT, rises from ~20 to ~45 °C, V increases drastically to ~160 mV, with an average dV/dT in this temperature range around 6 mV/°C. The average dV/dT in the entire temperature range, defined as V_{max}/T_{max}, is ~3.6 mV/°C, with V_{max} being the highest output voltage. The nonlinearity may come from the inherent ion structure in solid phase, as well as the confinement effects of nanopore walls—When the temperature is relatively high, diffusion of solvated ions along the axial direction in a nanopore can be accelerated, which promotes charge exchange between the inner surfaces of electrode and the bulk electrolyte solution phase; diffusion along the radius direction of a nanopore normal to the electrode inner surface is less affected [20, 27, 28].

For the NiNC-based TCS cell, the degree of nonlinearity of the V–T relationship is lower. As T increases from T_r to ~40 °C, V is about 10 mV; as T further rises to ~75 °C, V_{max} reaches ~100 mV. The overall dV/dT is ~2 mV/°C, somewhat lower than that of NiCNT-based cell, yet still much higher than that of TCS formed by neat carbon electrodes, ~0.65 mV/°C [11, 12]. It is clear that the high thermal sensitivity should be attributed to the Ni plating. The difference between the NiCNT and the NiNC systems may be associated with the impurities, e.g., Sn, the residual defects, and the configuration of nanopores.

We observed an electrode potential shift in NiCNT after high-temperature cycling between 25 and 126 °C, while pure Ni plate was quite thermally stable. This may be attributed to the impurities in Ni coating, which cause thermally enhanced galvanic surface reactions.

When the cell temperature is maintained at T_{max}, switch "S" is closed and the electrode and the counter-electrode form a circuit. Electrons move from the low-potential end to the high-potential end through the resistor, R_0; counter-charges move in the electrolyte solution between counter-electrode and electrode to complete the return path. The generated electrical energy by the TCS cell, i.e., the work dissipated by R_0, is converted from a portion of the thermal energy absorbed by the system. As a new equilibrium is approached at the electrode–electrolyte interfaces, the potential difference between them is lowered and would eventually converge to zero, as shown in Fig. 4. For self-comparison purpose, the time constant of voltage decrease, τ, is defined as the duration for V to decrease by a factor of e, the Euler's number. For the NiCNT-based system, τ is ~15 min; for the NiNC-based system, τ is ~2 h. The relatively long time constants should be related to the large electrode surface area and thickness: Because at the inner electrode surfaces, the solvated ions are confined by the nanopore surfaces from the radius direction, the ions must diffuse along the axial direction to move away or approach the interface double layer [29–33]. The diffusion distance is determined by the characteristic length scale of the electrode structure. The length of the MWCNT is around a few μm; the grain size of the nanoporous carbon is tens of μm, which explains why the time constant of the former is much shorter. After the time constant is reached, further reduction in voltage is increasingly slow, as the driven force of ion diffusion is reduced at the near-equilibrium condition. It takes ~14 h and nearly 2 days for the NiCNT and the NiNC systems to fully discharge, respectively.

The specific energy generated in each thermal cycle by the TCS system can be calculated from the data in Fig. 4 as $U = (1/m)\int (V^2/R_0)dt$, where t denotes time and m is the electrode mass. With a relatively small temperature change $\Delta T \approx 45$–50 °C, the values of U are ~600 and ~1800 mJ/g for the NiCNT system and the NiNC system, respectively; both are much higher than the target energy level ~50 mJ/g. It can be seen that although the NiCNT system exhibits a higher output voltage, because the NiNC system has a much larger specific surface area, the specific energy of the latter is higher by three times.

4 Concluding remarks

In summary, we developed thermally chargeable supercapacitor (TCS) systems based on nickel-coated carbon nanotubes and nanoporous carbon electrodes. The counter-electrode is a pristine nanoporous carbon. The system works with a homogeneous but changing low-grade heat source, without any temperature gradient. Thermal energy is absorbed and partially converted to electrical energy when the temperature increases; and the system configuration can return to its initial condition as temperature is reduced. That is, the energy harvesting is performed cyclically as temperature fluctuates. The experimental data indicate that, with the high work function of nickel, the electrode potential is highly thermally sensitive. As temperature increases, because the temperature dependences of the electrode and the counter-electrode are different, a net output voltage is generated. The large specific electrode surface area leads to a large energy density. The thermal sensitivity of electrode potential is around 3–6 mV/°C; with a temperature range of 45–50 °C, the harvested electrical energy is 600–1800 mJ per gram of electrode material per thermal cycle. The time constant of voltage decay is nearly proportional to the electrode surface area,

ranging from 15 min to 2 h for the systems under investigation. This result sheds light on the development of advanced energy harvesting devices of low-grade heat.

Acknowledgments The experimental research was supported by the National Science Foundation under Grant No. ECCS-1028010. The data analysis was supported by the Advanced Research Projects Agency–Energy under Grant No. DE-AR0000396.

References

1. B.F. Tchanche, G. Lambrinos, A. Frangoudakis, G. Papadakis, Low-grade heat conversion into power using organic Rankine cycles–a review of various applications. Renew. Sustain. Energy Rev. **15**, 3963–3979 (2011)
2. G. Nolas, J. Sharp, H. Goldsmid, *Thermoelectrics: Basics Principles and New Materials Developments* (Springer, Berlin, 2001)
3. T. Wang, Y. Zhang, Z. Peng, G. Shu, A review of researches on thermal exhaust heat recovery with Rankine cycle. Renew. Sustain. Energy Rev. **15**, 2862–2871 (2011)
4. W. Husband, A. Beyene, Low-grade heat-driven Rankine cycle, a feasibility study. Int. J. Energy Res. **32**, 1373–1382 (2008)
5. R. Lasseter, P. Paigi, Microgrid: a conceptual solution, in *35th Annual IEEE Power Electronics Specialisrs Conference* (2004), pp. 2521–2525
6. D. Tanner, Ocean thermal energy conversion: current overview and future outlook. Renew. Energy **6**, 367–373 (1995)
7. D.L. Ermak, R.A. Nyholm, P.H. Gudiksen, Potential air quality impacts of large-scale geothermal energy development in the Imperial Valley. Atmos. Environ. **14**, 1321–1330 (1980)
8. F.L. Curzon, B. Ahlborn, Efficiency of a Carnot engine at maximum power output. Am. J. Phys. **43**, 22–24 (1975)
9. I. Sur, A. Casian, A. Balandin, Electronic thermal conductivity and thermoelectric figure of merit of n-type PbTe/$Pb_{1-x}Eu_xTe$ quantum wells. Phys. Rev. B **69**, 035306.1-7 (2004)
10. Y. Qiao, V.K. Punyamurtual, A. Han, H. Lim, Thermal-to-electric energy conversion of a nanoporous carbon. J. Power Sources **183**, 403–405 (2008)
11. H. Lim, C. Zhao, Y. Qiao, Performance of thermally-chargeable supercapacitors in different solvents. Phys. Chem. Chem. Phys. **16**, 12728–12730 (2014)
12. H. Lim, W. Lu, X. Chen, Y. Qiao, Effects of ion concentration on thermally-chargeable double-layer supercapacitors. Nanotechnology **24**, 465401.1-5 (2013)
13. H. Lim, W. Lu, Y. Qiao, Dependence on cation size of thermally induced capacitive effect of a nanoporous carbon. Appl. Phys. Lett. **101**, 063902.1-4 (2012)
14. H. Lim, W. Lu, X. Chen, Y. Qiao, Anion size effect on electrode potential in a nanoporous carbon. Int. J. Electrochem. Sci. **7**, 2577–2583 (2012)
15. Lim H, *Recycling of Wasted Energy: Thermal to Electric Energy Conversion*. Ph.D. Thesis, University of California, San Diego, 2011
16. S.W. Lee, Y. Yang, H.W. Lee, H. Ghasemi, D. Kraemer, G. Chen, Y. Cui, An electrochemical system for efficiently harvesting low-grade heat energy. Nat. Commun. **5**, 3942.1-6 (2014)
17. Y. Yang, S.W. Lee, H. Ghasemi, J. Loomis, X. Li, D. Kraemer, G. Chen, Charging-free electrochemical system for harvesting low-grade thermal energy. Proc. Natl. Acad. Sci. **111**, 17011–17016 (2014)
18. T. Brousse, P.L. Taberna, O. Crosnier, R. Dugas, P. Guillemet, Y. Scudeller, P. Simon, Long-term cycling behavior of asymmetric activated carbon/MnO_2 aqueous electrochemical supercapacitor. J. Power Sources **173**, 633–641 (2007)
19. S.E. Larsen, J. Højstrup, C.H. Gibson, *Fast-Response Temperature Sensors. Air-Sea Interaction* (Springer, Newyork, 1980), pp. 269–292
20. T. Kim, W. Lu, H. Lim, A. Han, Y. Qiao, Electrically controlled hydrophobicity in a surface modified nanoporous carbon. Appl. Phys. Lett. **98**, 053106.1-3 (2011)
21. S. Arai, M. Kobayashi, T. Yamamoto, M. Endo, Pure-nickel-coated multiwalled carbon nanotubes prepared by electroless deposition. Electrochem. Solid State Lett. **13**, D94–D96 (2010)
22. H. Lim, Y. Shi, M. Wang, Y. Qiao, Effects of work function on thermal sensitivity of electrode potential. Appl. Phys. Lett. **106**, 223901.1-3 (2015)
23. J. Goodisman, *Electrochemistry: Theoretical Foundations* (Wiley, London, 1987)
24. LF Deis, *CRC Handbook of Chemistry and Physics*, (CRC Press, Boca Raton, FL, 2009)
25. X. Lang, A. Hirata, T. Fujita, M. Chen, Nanoporous metal/oxide hybrid electrodes for electrochemical supercapacitors. Nat. Nanotechnol. **6**, 232–236 (2011)
26. A. Gunawan, C.H. Lin, D.A. Buttry, V. Mujica, R.A. Taylor, R.S. Prasher, P.E. Phelan, Liquid thermoelectrics: review of recent and limited new data of thermogalvanic cell experiments. Nanoscale Microscale Thermophys. Eng. **17**, 304–323 (2013)
27. W. Lu, T. Kim, C. Zhao, X. Chen, Y. Qiao, Modified infiltration of solvated ions and ionic liquid in a nanoporous carbon. Appl. Phys. A Mater. Sci. Proc. **112**, 885–889 (2013)
28. W. Lu, A. Han, T. Kim, Y. Qiao, Effect of 16-mercaptohexadecanoic acid modification on liquid transport in a nanoporous carbon. Appl. Phys. Lett **94**, 223120.1-3 (2009)
29. V.K. Punyamurtula, A. Han, Y. Qiao, An experimental investigation on a nanoporous carbon functionalized liquid damper. Phil. Mag. Lett. **86**, 829–835 (2006)
30. V.K. Punyamurtula, Y. Qiao, Hysteresis of sorption isotherm of a multiwall carbon nanotube in paraxylene. Mater. Res. Innov. **11**, 37–39 (2007)
31. B. Xu, X. Chen, W. Lu, C. Zhao, Y. Qiao, Non-dissipative energy capture of confined liquid in nanopores. Appl. Phys. Lett **104**, 203107.1-4 (2014)
32. H. Li, X. Xu, Y. Qiao, An experimental investigation on fluidic behaviors in a two-dimensional nanoenvironment. J. Appl. Phys. **114**, 044302.1-6 (2013)
33. Y. Qiao, X. Xu, H. Li, Conduction of water molecules through graphene bilayer. Appl. Phys. Lett **103**, 233106.1-3 (2013)